Cooperative Autonomy of Multiple Solar-Powered Thermalling Gliders ⋆

Nahum Camacho, *
Vladimir N. Dobrokhodov, Kevin D. Jones, **
Isaac I. Kaminer ***

* *Graduate student at the Department of Mechanical and Aerospace Engineering, Naval Postgraduate School, Monterey, CA 93943 USA (e-mail: ncamacho@nps.edu)*
** *Research Associate Professors at the Department of Mechanical and Aerospace Engineering, Naval Postgraduate School, Monterey, CA 93943 USA (e-mail: vndobrok, kdjones@nps.edu)*
*** *Professor at the Department of Mechanical and Aerospace Engineering, Naval Postgraduate School, Monterey, CA 93943 USA (e-mail: kaminer@nps.edu)*

Abstract: In this paper a brief review of the multidisciplinary systematic approach to the the design of a fleet of cooperative gliders capable of extended endurance operation is presented. The flock of autonomous gliders is able to harvest energy from the environment, both through photovoltaic energy generation and through exploitation of natural convective lift in the surrounding air, and act cooperatively to meet mission requirements and to share knowledge of the local environment. The paper begins with a brief overview of the total-energy approach required for such a feat, along with a short description of key system components and the principal technologies. This is followed by details of the evolution of a previously-developed architecture that supported autonomous thermaling, to an architecture that considers the total-energy budget in all flight segments, and utilizes the cooperative flight to maximize the cumulative energy capture while simultaneously meeting mission objectives.

Keywords: cooperative control; solar energy; convective thermals energy; autonomous glider.

1. INTRODUCTION

One of the most critical limiting factors impacting effective collaborative autonomy today is the lack of endurance that is typical in most of the existing autonomous aircraft. Numerous futuristic ideas and concepts will not be implemented in real life solely due to this reason. Until *R&D* community realizes that the energy onboard (of either a single or a flock of agents) and the mission objectives are equally important metrics of the mission management (planning and execution), and finds a way of solving this challenge, there will not be revolutionary advances made in the area of persistent intelligent collaborative autonomy.

Despite almost two decades of significant advances in low-power and high-performance microelectronics development including CPUs, sensors, actuators, and communication circuits Tong [1995], Singh and Shukla [2010], the only task addressed was to lower the power consumption of autonomous machines and therefore to reduce the pace of energy expenditures. On the other hand, the progress of energy renewable technologies is lagging behind. Since the loss of energy is unavoidable due to the limited efficiency of energy conversion, storage, and transmission, the mission duration will always be limited. However, implementing novel approaches for the cooperative mission design and execution along with the optimal energy management can not only further reduce the rate of loss of limited onboard energy, but also can result in energy increase during the autonomous mission execution; this capability is not readily available today in any of the available technologies, see Siciliano and Khatib [2008], Martinez et al. [2008], and Nonami et al. [2013].

Despite the complexity of the energy-management task, the practical solutions of the extended duration flight do exist in nature. Millions of years of evolution enable a number of families of birds for very long duration flights. While the fundamentals of flight are the same, the effective energy management principles during the flight do differ. One of the most extraordinary birds capable of the long duration flight is the bar-tailed godwit, a large, streamlined shorebird, that performs a non-stop across the ocean flight, seeUSGS [2007], of more than eight days over a distance of 7,200 miles; the distance equivalent of making a round-trip flight between New York and Paris without ever touching down. Another example is the albatross that can fly around the world with little or no flapping of their wings, see Richardson [2011]. Remarkably, some birds can

⋆ The project has been supported over the last 3 years by a number of sponsors including the NPS Consortium for Robotics and Unmanned Systems Education and Research, the Army Research Lab, and the "The Multidisciplinary Studies Support for USMC Expeditionary Energy Office" program.

remain aloft for years at a time; the swift, for example, spends nearly its entire life in the air while landing only to breed. Along with many other animals (for example dolphins, whales), swifts evolved to be able to put one side of their brain to sleep at a time, so that they can sleep in the air while not actually being unconscious, see Lapierre et al. [2007]. What is common among these examples is not only the evolved capability of the high efficiency flight, but also the unique ability to manage energy that is implemented by both the optimal energy expenditures and energy harvesting.

Considering the state of the art in aerial robotics (algorithmic support, instrumentation, size weight and power (SWAP) constraints), it is our firm belief that the best approach to enable long duration flight would combine the collaborative mission management and energy harvesting. Collaboration is the first key capability that spans across every element of the mission. First, collaboration enables effective search for available energy sources. Most of the available energy sources are not visible but detectable by intelligent robots equipped with appropriate sensors. Thus, multiple agents would have much better chances of finding "free energy" when cooperating and sharing their findings. Second, the operational utility of multiple agents equipped with complementary sensors is superior to the capability of an individual agent. Finally, robustness of the collaborative mission execution is significantly higher because partial loss of a subset of the vehicles does not lead to the loss of entire flock capability. Energy harvesting and storage is the second complementary enabler of long endurance flight that allows for the accumulation of energy. The feasible methods of energy extraction in aerial application include the solar photovoltaic and airflow soaring; the soaring can be based on the convective air (thermaling) or wind shear energy extraction. While the photovoltaic boost can be achieved only during the daylight, the extraction of power of surrounded moving air can be utilized even during the nighttime. This combination is the ultimate solution for the "eternal" operational endurance.

Therefore, it is envisioned that enhancing mission performance while reducing its cost can be achieved by implementing the energy harvesting and collaboration capabilities onboard of multiple autonomous solar-powered and thermal-soaring gliders. Thus, the triplet of (***i***) mission management, (***ii***) energy harvesting and (***iii***) collaboration builds the fundamental architecture of future energy enhanced autonomy.

Since the number of involved algorithms and technologies is significant, the remainder of the paper briefly outlines the core ideas implemented to date in both the high-fidelity simulation and the real onboard hardware environments. Therefore, the section 2 describes the "individual gliders" algorithms as outline above. The following section 3 outlines the development of the collaborative autonomy algorithms. Section 4 provides details of the developed high-fidelity simulation environment used for verification and validation of the algorithms. The paper ends with a brief outline of the future development steps.

2. ALGORITHMS OF INDIVIDUAL GLIDERS

The algorithms of individual platforms are primarily responsible for the sustainable flight of a partially uncertain glider and exploration and sharing of knowledge about the environment. The algorithms run online and enable identification of the inherent flight dynamics properties of the glider which are in turn used to detect the thermal updrafts. When flying in the updraft the guidance algorithm is engaged to enable the maximum harvesting efficiency of the updraft's energy, and on the other hand estimates the updraft geometry and motion that are used to georeference the updraft and share its utility properties across the network of collaborative gliders. Besides the collaborative mission objective and initial mission plan, the georeferenced map is the formalized knowledge used in the collaborative mission replanning phase. While in autonomous soaring mode, the electrical management system that consists of solar panels, batteries and the maximum energy tracking circuitry, supports the avionics and recharges the batteries keeping them evenly balanced. At any given time each individual platform can be either in a search or in a soaring mode. While the soaring mode is primarily defined by the energy gain objective, the search mode is driven by the intelligent algorithm that combines the goals of the distributed mission and the need to search for energy sources in the environment. Development of these intelligent onboard components that enable optimal balancing of energy gain and mission objectives is the most promising direction of the current and future research.

2.1 Electric Energy Management Subsystem

As mentioned above, there are two sources of energy input into the system: photovoltaic and atmospheric convection, and typically two methods of energy storage; potential energy stored chemically in batteries and potential energy stored via altitude. This section describes the electrical half of that system; electricity harvesting through photovoltaic conversion and energy storage in rechargeable batteries.

Earlier it was mentioned that solar radiation could be given empirically for a given location and time of year. This provides an estimate of what energy-density might be available from solar radiation. Knowing an array size, cell efficiency, and with estimates of air clarity, an estimate for available energy input from the array over a 24-hour period may be made. The current glider is outfitted with research-grade mono-crystalline Silicon cells with an advertised efficiency of 22.5%. The cells are semi-rigid - they don't qualify as flexible, but they can very carefully be bent to conform to the airfoil surface over the majority of the wing. Ideally, as much of the aircraft surface as possible should be covered by the array, but it must be done in such a way that it does not disturb the boundary layer. While the system may gain energy through the array, it won't help if the aircraft loses that same energy through increased viscous drag or loss of lift. Therefore, the cells are built into the wing surface during initial composite lay-up of the wing, such that they are essentially conformal, with only subtle fine-texture differences. A small section of wing with embedded cells is shown in Fig. 1.

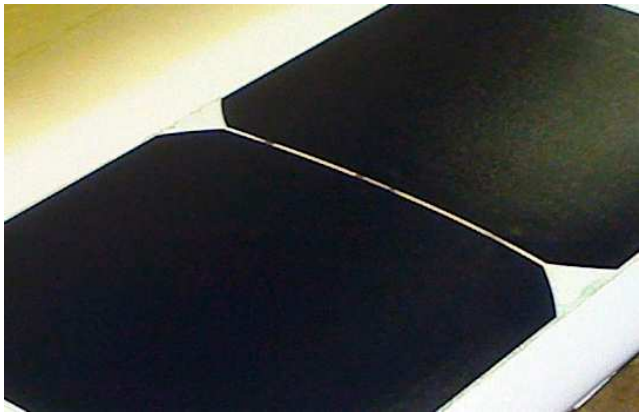

Fig. 1. Sample wing section with conformal, embedded cells.

In the current generation of the aircraft, a small solar array has been included in order to identify aerodynamic and structural issues that might arise. For example, the solar cells get quite hot while the aircraft is at rest on the ground. Will this heat be sufficient to damage the wing structure by softening the epoxy resin used in the composites, or delaminate the protective film around the cells? When the wing flexes in flight, will this damage the semi-rigid cells or break them loose from the wing? The current array includes 18 cells for an array area of 0.28 m^2. With the estimates for efficiency, this should provide on the order of 440 Wh in a 24-hour period in June, or roughly 50 W at mid day.

Photovoltaic cells operate with variable output voltage and current which is dependent on the available radiation and the load impedance. In order to maximize power output, circuitry is required to actively adjust the load impedance to drive the product of voltage and current (power) to a peak. This device is called a Maximum Peak Power Tracker, or MPPT. The MPPT circuit uses switching circuitry which is typically combined with a buck or boost converter to yield a regulated DC voltage output. There is an efficiency associated with the MPPT, but it is typically quite high, typically better than 99 percent.

The power coming from the MPPT is split and is fed into a charge controller for the batteries and to the load (avionics, propulsion, payload). If the power coming from the MPPT is greater than the load, it is used to charge the batteries, storing potential energy for later use. If the load is greater than the power coming from the MPPT then it taps into the batteries, depleting stored potential energy.

Battery selection is the next challenge. Typically Lithium-chemistry batteries have the highest *energy-density* for commercially available rechargeable batteries, but there is an enormous variation from type to type. Most suitable cell technologies fall into two categories, the *can*-type cells usually found in laptops, and the foil-wrapped flat cells typically found in cell phones and other compact electronics. The can-type cells are usually referred to as Lithium-Ion or LiIon batteries, and the most common form-factor is the 18650 cell, which is nominally 18 mm in diameter and 65 mm long. These cells typically cannot support high discharge rates. Most are caped at a 1C continuous discharge rate, where the 1C rating means that the cell would be depleted in one hour. This equates to a low *power-density*. This limitation will likely not be a concern, as the batteries are intended to be used through the night, with average discharge rates of less than 0.1C. Depending on the pack size, this is a potential limitation when the motor is used, as it is a short-term, but very high load.

Table 1. Measured battery performance

Type	C-rate	Energy (Wh)	Energy Density (Wh/kg)
LiPo	0.209	115.5	177.7
LiPo	2.502	105.8	162.8
LiIon	0.171	107.9	167.3

The flat foil-wrapped battery type is usually referred to as Lithium polymer or LiPo. These are commonly used in cell phones and other compact devices as well as the radio control aircraft hobby. Unlike the LiIon cells, the power-density of LiPo cells can be extremely high. Many in the hobby industry claim continuous discharge rates of 70C with bursts of up to 140C. This equates to draining the battery in less than one minute. Unfortunately, there is an inverse relationship between energy-density and power-density in these cells. In order to achieve the high discharge rates, the cells need more copper to carry the current, and the cells must be larger and heavier.

Analyzing manufacturer specification for the LiIon cells, energy densities in excess of 200 Wh/kg are frequently listed, whereas for the lower discharge-rate LiPos the highest is on the order of 190 Wh/kg. Samples of both cell types were tested in current project. The LiIon cells had an advertised capacity of 3 Ah, and an energy density on the order of 220 Wh/kg. The LiPo cells had an advertised capacity of 2 Ah, and an energy density of just over 190 Wh/kg. Experiments were set up to test the cells under typical loads. Twelve LiIon cells were formed into a pack of 4 cells in series (4S) and 3 cells in parallel (3P), to make a 4S3P pack with a nominal voltage of 14.8 V and capacity of 9 Ah. Sixteen LiPo cells were formed into a 4S4P pack with nominal 14.8 V and 8 Ah capacity.

Due to internal cell resistance, the usable energy in the packs is a function of discharge rate. The LiPo pack was tested at two discharge rates, 0.21C and 2.51C, with voltage and current logged from start to finish. The LiIon pack cannot support the higher discharge rate, but was tested at a lower 0.17C rate. Results of the discharge tests are shown in Figs. 2 and 3, plotting voltage and energy-use as functions of normalized discharge time, respectively. As with most batteries, voltage slowly drops over the discharge cycle, a feature that is convenient for estimating remaining energy in the pack. The voltage also drops as a function of load, which is a result of the internal cell resistance and Ohm's law.

The discharge cycles were halted when the pack voltage reached 3.2 V/cell or 12.8 V for the pack. For the LiPo pack this is considered to be the lowest, safe voltage for the cells, The LiIon packs can typically be safely drained to a lower voltage, although it is apparent from Fig. 2 that the voltage has already dropped off the cliff, and there is very little actual energy left in the pack. The measured useful pack energy and energy-density are shown in Table 1.

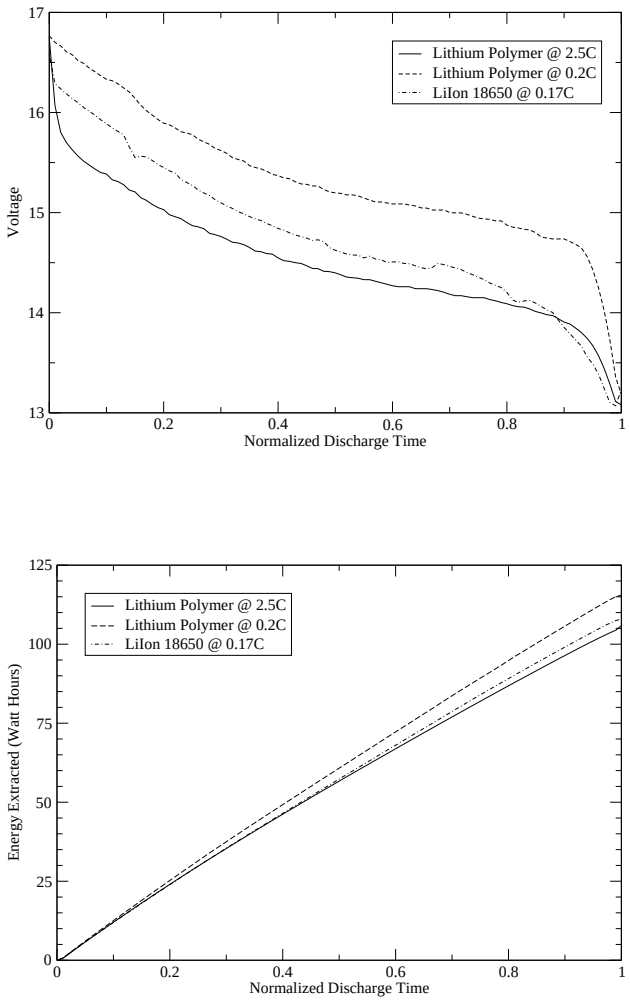

Fig. 3. Energy-out as a function of normalized discharge time.

The sensitivity to drain rate is clear. Also clear is the fact that advertised energy and energy-density might not be achievable in a practical application. While the LiIon cells would appear to be far superior based on manufacturers' specifications, experiments would tend to suggest that LiPo batteries are superior for this project.

Battery capacity is driven by the need to survive the night with no photovoltaic energy input. At a minimum the battery must power the avionics and payload components that are in use. Thermal activity will diminish at night, although the same algorithm that exploits thermal lift during the day may be used to minimize sink during the night. If there are pockets of air that sink, there must be pockets of air that rise. The lift may be weak, but better than no lift at all. When the lift is insufficient to maintain altitude, the motor must be used to regain it.

Use of the motor for propulsion introduces additional efficiency considerations. The motor is a sensorless brushless motor with electronic speed control. Motor efficiencies are quite high at nominal power settings. All brushless motors have internal resistance and a parameter called I_0 that represents the no-load current at a specific voltage. These two terms dictate the efficiency of the motor over its useful power spectrum. With no load they will draw power from the system that is roughly $I_0 * V$ and at an efficiency of zero. As the mechanical load is increased, the efficiency rapidly increases to some peak value. While the motor might have a nominal efficiency of better than 90 percent at its rated power, at a much lower power the efficiency can be very low, perhaps below 50 percent. This becomes critical when the motor is used for propulsion. The current airframe at nominal weight requires on the order of 40 W to sustain cruise flight, but the motor is rated for up to 1000 W. At full throttle with the included gear drive and propeller it draws on the order of 400 W with an estimated total efficiency in excess of 85 percent, but at 40 W the system efficiency is down around 10 percent. This is a clear indication that when the motor is used, it should be used at a high power setting, not to sustain cruise flight, but to actively gain altitude, using elevation as energy storage. The intermittent high power draw from the propulsion will reduce the battery efficiency somewhat, but this is much more subtle than the motor efficiency curve.

2.2 Glider Identification and Updraft Detection

There is a number of prior efforts devoted to the autonomous soaring capability. First demonstrated by human pilots in 1900s (see Simons and Schweizer [1998]) the idea of soaring in convective air became feasible for onboard autonomous implementation only in the 1990s, see Wharington [1998]. While enabling the desired functionality by primarily mimicking the birds flight and indeed achieving significant extended flight capabilities (see Edwards [2008], Allen [2006] and Allen and Lin [2007]), most of the algorithms use heuristics in the identification of the updraft strength, its potential utility in energy gain, and the decision of when and how to enter the updraft. The reason for employing heuristic approaches is obvious, since both the strength of the updraft and its efficiency are both subject to significant uncertainties. First, they result from the uncertain flight characteristics of the specific glider no matter how well the airframe is modeled and flight tested; significant advances in material and structures sciences produce novel airframes that are strong and flexible on one hand, and therefore aerodynamically uncertain when bend and twisted on the other hand. Second, when a glider is propelled through the unsteady air the updraft estimation algorithm lacks spatial content (both in horizontal and vertical directions) in the noisy measurements of the vertical velocity of convective air. Thus, for any given altitude of flight it takes essential time before the updraft geometry is identified and the guidance algorithm is engaged. It is worth noting, that when controlled by the thermal centering guidance law the estimation algorithm partially regains the spatial data in horizontal direction. To successfully identify the thermal strength in vertical direction it would take prohibitively long time for a single glider, thus to achieve rapid identification of $3D$ energy profile of any given thermal updraft it is very effective to utilize a number of collaborative platforms simultaneously sampling the same updraft in three dimensions.

The approach used in our development shifts the focus from heuristics toward the online estimation of the glider flight dynamics and the parameterized model of the convective updraft. The algorithm of detecting a thermal is based on combining two complementary approaches.The

first approach utilizes the inherent sink rate polar and the second one is based on the total energy of the system.

Precise characterization of the sink polar (the function of vertical sink rate versus the true airspeed (TAS) of the platform) of a particular glider can be practically achieved in extensive experimentation. However, flight-experimentation in the real-world environment can hardly provide ideal controlled conditions, and in every flight of the same platform there are always subtle differences that cannot be accounted for. Estimates of the sink-polar were made by post-processing a collection of experimental flight results obtained in low-wind, low-lift conditions, see Andersson et al. [2012b]. Sink polars are roughly quadratic in nature, and a least-squares approach yields suitable coefficients based on the historical data. In flight, a recursive linear least square (RLLS, see Astrom and Wittenmark [1975]) estimator may be used in real-time to account for specific variation in the platform and atmospheric conditions at that moment. An example of this approach is shown below in Figure.4 for a full-scale ASW-27 glider using the Condor simulator (Condor [2013], see details in in sec.4) for the real-time flight data source.

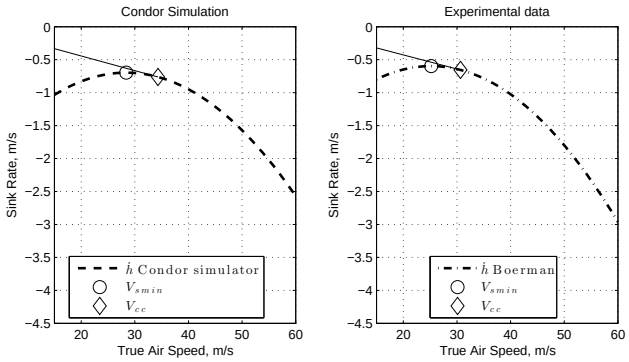

Fig. 4. Identifying the inherent sink polar: both the sink rate and the TAS are directly measured by the on-board sensors. Minimum sink rate V_smin and the optimal crusing speed V_{cc} corresponding to the maximum glide ratio (typical for the "cross-country" flight) are presented.

The analytical representation of the sink polar significantly contributes not only to the identification of thermal updrafts but also to the mission planning of a specific glider, see Piggott [1997] and FAA [2011]. In particular, the polar defines the minimum sink rate V_smin and the corresponding TAS command for the autopilot to follow. While V_smin may be too close to the stall speed V_{stall} and should be avoided ($V_{stall} \approx V_smin$), the effective speed commanded in thermaling mode V_{th} may be slightly higher. The polar also defines the optimal TAS command V_{cc} for the maximum glide ratio flight that is used by the navigation task in planning for the maximum range "cross-country" segment. While the sink polar is ideally obtained in no-wind environment, its application to the known wind conditions is also straightforward and allows for the calculation distances to be traveled in cross-country flight, see more details in Piggott [1997] and FAA [2011].

The total energy approach is also widely used in human piloted soaring flight. It is based on the concept that at any given time the mechanical energy E_{tot} of the soaring glider combines the potential energy, $E_p = mgh$, and kinetic energy, $E_k = \frac{m \cdot V^2}{2}$, of the airframe minus the "leakage" of the energy due to the work of the parasitic and induced aerodynamic drag, E_D. For an aerodynamically "clean" glider with an objective to minimize the total energy loss, the control commands of its autopilot will necessarily result in mild variations of the angle of attack, thus leading to the relatively constant parasitic drag and $\dot{E}_D \approx 0$. Consequently, for the total energy and its rate of change over sufficiently long time intervals one can consider the following:

$$E_{tot} = mgh + \frac{m \cdot V^2}{2} - E_D, \quad E = \frac{E_{tot}}{mg},$$
$$\dot{E} = \dot{h} + \frac{V \cdot \dot{V}}{g}, \quad \ddot{E} = \frac{\dot{V}^2 + V \cdot \ddot{V}}{g} + \ddot{h}, \qquad (1)$$

where m is the mass of the airframe, g is the gravitational constant, E is the normalized total mechanical energy of the system (also called the specific energy), h is the height, and V is the inertial speed. Therefore, for highly efficient airframes the longitudinal long period oscillations represent the natural tradeoff of kinetic and potential energy while their sum remains nearly constant. As a consequence, in no updraft conditions the rate of change of the total energy $\dot{E} \approx 0$. Therefore, if there is a significant variation of the total energy, then the energy rate will be significantly away from zero thus indicating the energy variation due to updraft or downdraft airflow. In fact, the total energy management just presented is widely used in manned aviation being implemented in the so-called total energy compensating (TEK) variometers, see for example PitLab [2013].

All the components of equation (1) are readily available in onboard autopilot. Both equations in (1) are included into one Kalman filter along with the inertial and barometric sensors outputs. The resulting energy rate based solution provides another precise indication of the updraft event. A comparison of the outputs of both approaches with the output of the TEK variometer $\dot{h}_{TEK}$ is presented next in Figure.5.

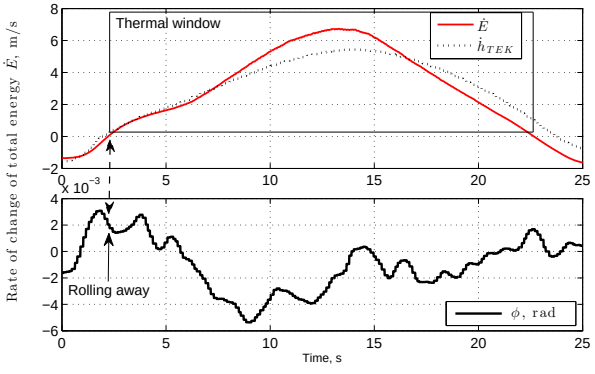

Fig. 5. Comparison of two approaches to the detection of thermal updrafts in mathematical model using Condor flight simulator, see Condor [2013].

The outcomes of the total energy estimator in (1) are used in the guidance law implementation that is presented next.

2.3 Guidance in Thermal Centering Mode

When a thermal updraft is detected the glider needs to perform an automatic maneuver to enable staying in the thermal with the objective of increasing the glider's potential energy through a rapid increase of the height. The theoretical development of the thermaling guidance law has been recently reported in Andersson et al. [2012b]). The most recent experimental results and findings that motivate further refinement of the solution were discussed in Andersson et al. [2012a]. This development was recently modified to include explicitly the sign of the turn rate command that is defined by the estimate of the body roll rate $\hat{p}$; it was observed in a number of flights that entering the thermal induces the motion that rolls the wings away from the thermal, thus suggesting the turn in an opposite direction. The resulting thermaling guidance law implemented onboard of real glider enabled successful latching and effective exploitation of the thermal.

The thermal centering guidance law that produces a turn rate command $\dot{\psi}_c$ to the autopilot is based on the feedback control law that takes into account the desire to get closer to the updraft (defined by the ρ_d) where its intensity (the vertical speed) is the highest, while balancing the turn rate and the turn-induced sink rate by a measure proportional to the rate of change of the total energy increase (defined by the $\ddot{E}$ in (1)), see the geometry of the guidance task in Figure.6 and the resulting guidance law in (2):

$$\dot{\psi}_c = -sign(\phi) \cdot (\frac{V}{\rho_d} - k_1 \cdot \ddot{E}), \qquad (2)$$

where ρ and ρ_d are the current distance and the desired orbital radius around the center of the thermal updraft, ϕ is the roll angle induced by the updraft, and k_1 is the feedback gain defined by the stability and performance requirements. For the feasibility of theoretical development

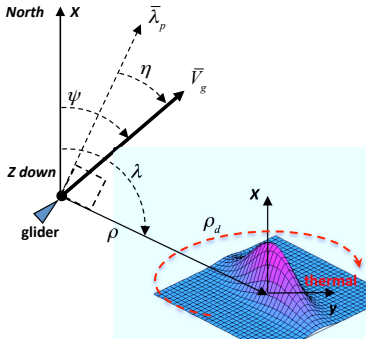

Fig. 6. Kinematics of guidance around a thermal updraft; the desired orbit is represented by the red dashed line defined by ρ_d.

the thermal center is assumed stationary with its position unknown. The desired distance (ρ_d) toward the center at this point is not defined, however for the stability of the control law it is assumed to be away from zero. The best value of ρ_d is initially assigned based on statistical observations of the glider performance and the shapes of updrafts in the area. Later on when collaborative gliders contribute to the identification of the updraft geometry this value is updated, thus resulting in a feedback that improves the collaborative efficiency of utilizing the free energy of the updraft. For the stability analysis of the thermaling guidance law it is assumed that the intensity of the updraft can be represented by the Gaussian distribution function of the form:

$$\omega = \omega_p \cdot e^{-[\frac{(x-x_0)^2+(y-y_0)^2}{2\sigma^2}]}, \qquad (3)$$

where x, y represent the coordinates of the glider, x_0, y_o represent the unknown coordinates of the center of updraft, ω_p is the peak intensity of the updraft,and σ defines the geometry of the symmetric updraft (in general case $\sigma_x \neq \sigma_y$). For a stationary updraft modeled by Gaussian distribution function with $\sigma > 0$, $\omega_p > 0$ and the glider with $V > 0, \rho_d > 0$ it is proven that the feedback guidance law in (2) is locally asymptotically stable with an equilibrium at $(\eta, \rho - \rho_d) = (0, 0)$ and a region of attraction $\Omega = \{(\eta, \rho - \rho_d) : |\rho - \rho_d| \leq \beta, |\eta| \leq \alpha\}$, where $\beta < \rho_d, \alpha < \pi/2$, for any

$$k_1 > \tan\alpha \frac{\sigma^2}{\omega_p(\rho_d - \beta)^2} e^{(\frac{-(\rho_d+\beta)^2}{2\sigma^2})}.$$

2.4 Identification of the Updraft Geometry

As described above, the thermal intensity model adopted for the stability analysis of the thermal centering guidance law is the 2-dimensional Gaussian distribution (3). Although its effective application was successfully demonstrated, it is realized, that the thermals geometry and their motion is more complex: it does not only move but also bends, see Reichmann and Bishop [1978] and the experimental result in Figure.7 obtained by a single glider persistently staying in an updraft, see Andersson et al. [2012b]. It can be argued whether Gaussian function is a good representation of a thermal or not. However, even if a Gaussian distribution does not encompass all the features of an actual updraft, most sources agree that it does capture many of the key characteristics of a real thermal, i.e., being strongest at the core, with a rounded shape and gradual decrease in strength towards the edges; see, for example, Wharington [1998] and Pagen and Bryden [1992]. At the end, the ultimate goal of the updraft identification is to develop a georeferenced map of thermals in the operational area to enable intelligent mission planning with an account of free energy resources.

3. COOPERATIVE ALGORITHMS

Our initial approach to the estimation of thermals ($2D$ coordinates of the center vs. the glider altitude) by utilizing the measurements of single glider in soaring mode was based on two classical nonlinear filtering techniques: first - the nonlinear Kalman filter with the "bearings only measurements", and second - the kinematic relation $\dot{\psi} = \frac{V}{\rho}$ between the speed over ground V and the turn rate $\dot{\psi}$, see Figure.6. In both formulations the bearing to the updraft center was assumed to be constant at $\pi/2$ ($\eta = 0$) with respect to the direction of flight being defined toward the center of the turn; the solution adopted the development in Dobrokhodov et al. [2008]. When entering a strong updraft, the filter performance was reasonable, resulting in a converging solution in about 2 full orbits

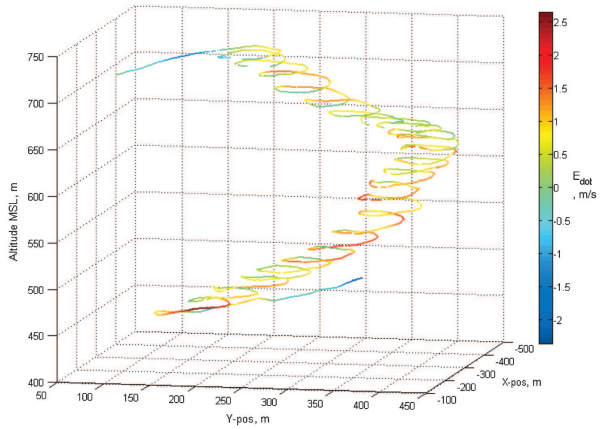

Fig. 7. The experimentally obtained shape illustrates complex geometry of an updraft; color coding represents the rate of change of the total energy (1) of a glider guided by the control law in (2).

and precision of the thermal center estimation of $75m$; the experimental setup unfortunately does not allow for true data of the thermal, while the simulation data is not a representative metric for the comparison.

3.1 Bayesian Mapping of Thermals

To increase the efficiency of online implementation the solution should integrate not only the knowledge gained by multiple gliders, but also the prior meteorological observations (see Pennycuick [1998], Hindman et al. [2007]), which might be available for the area of operation. Such data can be conveniently interpreted as a map of probability density of convective air activity with respect to the geographic latitude and longitude of the area of operation, see a conceptual example in Figure.8.

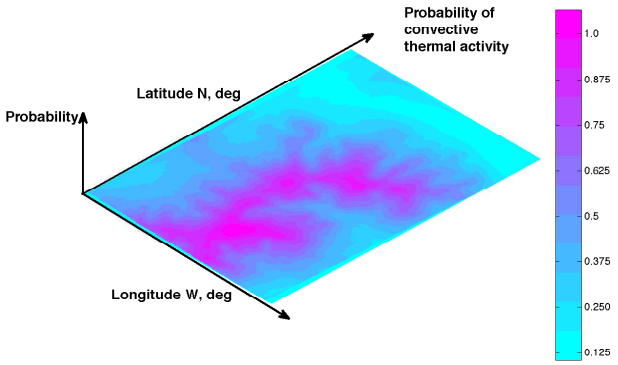

Fig. 8. "Heat map" of probability of finding a thermal over an area of operation.

As a first step toward cooperative identification and mapping of thermals over extended areas with an account of prior methodological observation, the probabilistic recursive Bayesian approach was adopted, see details of the approach in Bergman [1999].

Consider a task where N gliders cooperatively estimate the velocity $f_k = f(x_k, y_k, z_k, k)$ of flow field at the inertial coordinates x_k, y_k, z_k of k-th glider, $k = 1...N$. Assume that the onboard instrumentation enables measuring the lateral and vertical components of the airflow. The convective airflow of interest is captured by a given parametric model with unknown characteristics; see the vertical updraft model in (3) with unknown parameters $\omega_p, \sigma, x_0, y_0$. The objective of the task is to estimate f by cooperatively using noisy observations of the airflow.

Let $X(t) = (\omega_p, \sigma, x_0, y_0)$ be a state vector that encapsulates the unknown parameters of the convective flow velocity f_k that is estimated at each point of the discretized space at time t, $s_k(t)$ denote the noisy measurement of vehicle k at time t, and $S_k(t) = \{s_k(0), ..., s_k(t)\}$ define the set of samples up to the current time t. Assume that $s_k(t)$ of each vehicle at location x_k, y_k, z_k is corrupted by Gaussian noise such that $s_k(t) = f_k(x_k, y_k, z_k) + \mu_{h,k} + \mu_{v,k}$, with $\mu_{h,k} \sim N(0, \sigma_h^2)$ and $\mu_{v,k} \sim N(0, \sigma_v^2)$ being white noise components in horizontal and vertical directions.

Then the conditional probability of the state $X(t)$ given the set of measurements $S_k(t)$ of k-th glider is

$$P(X(t)|S_k(t)) = \beta \cdot P(s_k(t)|X) \cdot P(X(t)|S_k(t-1)), \quad (4)$$

where β is the normalization coefficient chosen to guarantee that $P(X(t)|S_k(t))$ at every instance of t has a unity integral over the state-space X. The $P(s_k(t)|X)$ is the likelihood function represented by the conditional probability of the measurement $s_k(t)$ given the state $X = f_k$, and the $P(X(t)|S_k(t-1))$ is the prior probability distribution that represents any prior knowledge or intelligence about the most likely location and intensity of thermals. In our development $P(X(t)|S_k(t-1))$ is what encapsulates the probability "heat map", see Figure.8.

Finally, let each point of state X in the state-space be represented by the multi-variate Gaussian likelihood function:

$$P(s_k(t)|X) = \frac{1}{[2\pi\Delta]^{\frac{1}{2}}} exp(\frac{-[f_k(X) - s_k(t)]}{\sum[f_k(X) - s_k(t)]}),$$

where $\Delta = diag(\mu_h^2, \mu_v^2)$. Assuming that measurements are taken at each time step and the gliders cooperatively share the data, the conditional probability density of the state $X(t)$ is updated through the natural motion of the fleet of gliders sampling the airflow at (x_k, y_k, z_k) as

$$P(X(t)|S(t)) = \beta \cdot \prod_{k=1}^{N} P(s_k(t)|X) \cdot P(X(t)|S(t-1)),$$

where $S(t-1)$includes the measurements from all N gliders in the fleet. Now it is clear that the points of the parameter space corresponding to the maximum of the posterior probability density $X(t) = maxP(X(t)|S(t))$ provide the best estimate (maximum likelihood) of the convective flow field parameters.

An example of the recursive Bayesian algorithm for the case of three simulated gliders cooperatively flying and estimating parameters of the same updraft is presented in Figure.9, for details see the simulation setup and the description of the experiment in section 4. In the demonstrated result the prior probability density is initialized by a uniform function that is defined as an inverse of the area

of operation. The result corresponds to the progression of the probability density function estimated by glider #1 along its flight path, see the corresponding cooperative trajectories of gliders #2 and #3 in Figure.10.

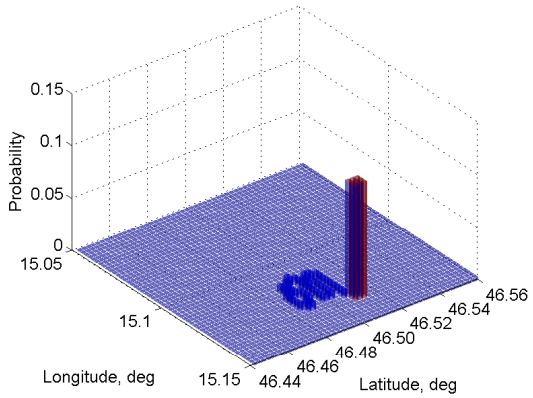

Fig. 9. Estimated location of an updraft obtained by glider #1 from the cooperative sampling of environment.

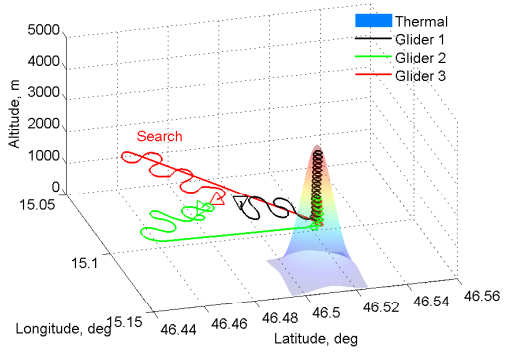

Fig. 10. An example of cooperative flight of three gliders; starting at different locations they all converge to the same updraft when glider #1 finds it and shares its estimated location.

4. SIMULATION ENVIRONMENT

To facilitate convenient design and verification of the designed algorithms the project also developed a realistic simulation environment that is based on tight integration of MatLab/Simulink capabilities with the high-fidelity flight dynamics and atmospheric effects of the Condor soaring simulator, see Condor [2013]. Besides providing a wide nomenclature of gliders, the software is capable of integrating the cooperative behaviors of human pilots that is essential to our project; the collaboration is enabled by sharing the states of gliders over the network. The architecture of the software in the loop (SIL) setup that integrates Condor with MatLab/Simulink is presented in Figure.11.

As an illustration of the achieved capabilities Figure.10 represents the cooperative flight of three gliders in a simplified scenario. The task is to find a single updraft in a bounded area and to converge to the same thermal by utilizing all the algorithms discussed above; the task

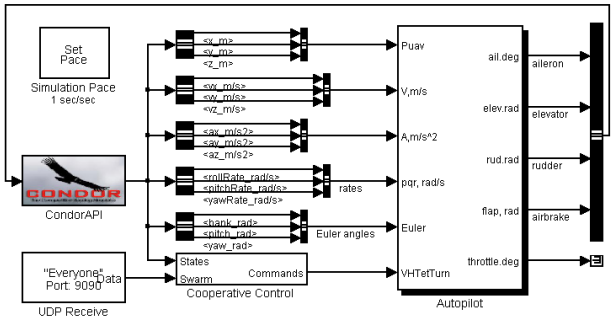

Fig. 11. Integration of Simulink and Condor capabilities in high-fidelity SIL environment.

mimics the setup and the objectives of our first cooperative flight test of two gliders reported earlier in Andersson et al. [2012b]. The gliders start their flight simultaneously at the same altitude and initially spend some time in exploring and searching for thermals. When glider #1 finds the updraft and shares the information about the estimated center of the thermal the other two gliders arrive to the same thermal and successfully gain height all together.

Time history of the altitude of three cooperative gliders is presented next in Figure.12. The result clearly demonstrated the benefits and significant potential of collaborative strategies in harvesting the convective updraft energy from the environment.

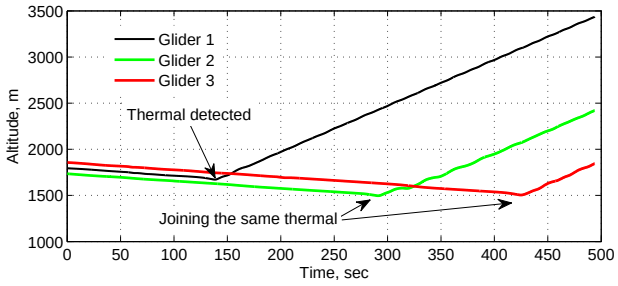

Fig. 12. An example of cooperative flight of three gliders; cooperative gain of altitude is the metric used here to evaluate the efficiency of developed strategies.

5. FUTURE WORK

The future plans include the development in two primary directions. First is the design of novel distributed approaches for effective environment sensing and energy harvesting along with the cooperative mission management and execution algorithms. We envision that in a typical mission with the goal defined by the waypoints in the area of operation, the task of finding an optimal route for multiple "traveling salesman" to visit all waypoints can be solved by weighting the edges of the underlying graph according to the proximity to the free energy sources in the area.

Second is to develop new hardware platform with high efficiency flexible solar panels integrated into the skin of the glider wings and the corresponding monitoring and the energy management algorithms. The task is underway with expected first flight of a single solar powered platform to be performed in February 2014.

ACKNOWLEDGEMENTS

The project has been supported by a number of sponsors including the NPS Consortium for Robotics and Unmanned Systems Education and Research, the Army Research Lab, and the "The Multidisciplinary Studies Support for USMC Expeditionary Energy Office" program. Besides these funding sources the authors would like to acknowledge the contribution of graduate students Andrew Streenan and Joshua Weiss for providing results of their final project and contributing to the extensive simulation research.

REFERENCES

Michael J Allen. Updraft model for development of autonomous soaring uninhabited air vehicles. In *Forty Fourth AIAA Aerospace Sciences Meeting and Exhibit*, 2006.

Michael J Allen and Victor Lin. Guidance and control of an autonomous soaring vehicle with flight test results. In *AIAA Aerospace Sciences Meeting and Exhibit, AIAA Paper*, volume 867, 2007.

Klas Andersson, Kevin Jones, Vladimir Dobrokhodov, and Isaac Kaminer. Thermal highs and pitfall lows-notes on the journey to the first cooperative autonomous soaring flight. In *Decision and Control (CDC), 2012 IEEE 51st Annual Conference on*, pages 3392–3397. IEEE, 2012a.

Klas Andersson, Isaac Kaminer, Vladimir Dobrokhodov, and Venanzio Cichella. Thermal centering control for autonomous soaring; stability analysis and flight test results. *AIAA Journal of Guidance, Control, and Dynamics*, 35(3):963–975, 2012b.

KJ Astrom and Björn Wittenmark. *Adaptive control*. Addison-Wesley, 1975.

Niclas Bergman. *Recursive Bayesian Estimation*. PhD thesis, Department of Electrical Engineering, Linköping University, Sweden, 1999.

Condor. The competition soaring simulator, October 2013. URL `http://www.condorsoaring.com/`.

Vladimir N Dobrokhodov, Isaac I Kaminer, Kevin D Jones, and Reza Ghabcheloo. Vision-based tracking and motion estimation for moving targets using unmanned air vehicles. *Journal of guidance, control, and dynamics*, 31(4):907–917, 2008.

Daniel J Edwards. Implementation details and flight test results of an autonomous soaring controller. In *AIAA Guidance, Navigation and Control Conference and Exhibit*. North Carolina State University, 2008. AIAA 2008-7244.

Federal Aviation Administration FAA. *Glider Flying Handbook*. JL Aviation LLC, 2011.

Edward Hindman, Stephen M Saleeby, Olivier Liechti, and William R Cotton. A meteorological system for planning and analyzing soaring flights in colorado usa. *Technical Soaring*, 31(3):68–82, 2007.

Jennifer L Lapierre, Peter O Kosenko, Oleg I Lyamin, Tohru Kodama, Lev M Mukhametov, and Jerome M Siegel. Cortical acetylcholine release is lateralized during asymmetrical slow-wave sleep in northern fur seals. *The Journal of Neuroscience*, 27(44):11999–12006, 2007.

David R Martinez, Robert A Bond, and M Michael Vai. *High performance embedded computing handbook: A systems perspective*. CRC Press, 2008.

Kenzo Nonami, Muljowidodo Kartidjo, Kwang-Joon Yoon, and Agus Budiyono. *Autonomous Control Systems and Vehicles: Intelligent Unmanned Systems*. Springer Publishing Company, Incorporated, 2013.

Dennis Pagen and B Bryden. *Understanding the sky*. Black Mountain Books, 1992.

CJ Pennycuick. Field observations of thermals and thermal streets, and the theory of cross-country soaring flight. *Journal of Avian Biology*, 29(1):33–43, March 1998.

Derek Piggott. *Gliding: A handbook on soaring flight*. A & C Black, 1997.

PitLab. Skyassistant variometer, October 2013. URL `http://www.pitlab.com`.

Helmut Reichmann and Max Bishop. *Cross-country soaring, Soaring Society of America*. Thomson Publications, 1978.

Philip L Richardson. How do albatrosses fly around the world without flapping their wings? *Progress in Oceanography*, 88(1):46–58, 2011.

Bruno Siciliano and Oussama Khatib. *Springer handbook of robotics*. Springer, 2008.

Martin Simons and Paul A Schweizer. *Sailplanes by Schweizer: A History*. Crowood Press, 1998.

Gaurav Singh and Sandeep Kumar Shukla. *Low Power Hardware Synthesis from Concurrent Action-Oriented Specifications*. Springer, 2010.

Ho-Ming Tong. Microelectronics packaging: present and future. *Materials chemistry and physics*, 40(3):147–161, 1995.

USGS. Bird completes epic flight across the pacific. ScienceDaily, September 2007.

John Wharington. *Autonomous control of soaring aircraft by reinforcement learning*. PhD thesis, Royal Melbourne Institute of Technology (Australia), 1998.